Correlated Fluorescence-Atomic Force Microscopy of Membrane Domains: Structure of Fluorescence Probes Determines Lipid Localization

James E. Shaw,*‡ Raquel F. Epand,§ Richard M. Epand,§ Zaiguo Li,¶ Robert Bittman,¶ and Christopher M. Yip*†‡

*Departments of Biochemistry, †Chemical Engineering, and Applied Chemistry, ‡Institute of Biomaterials and Biomedical Engineering, University of Toronto, Toronto, Ontario, Canada M5S 3G9; §Department of Biochemistry and Biomedical Sciences, McMaster University, Hamilton, Ontario, Canada L8N 3Z5; and ¶Department of Chemistry and Biochemistry, Queens College of the City University of New York, Flushing, New York 11367-1597

ABSTRACT Coupling atomic force microscopy (AFM) with high-resolution fluorescence microscopy is an attractive means of identifying membrane domains by both physical topography and fluorescence. We have used this approach to study the ability of a suite of fluorescent molecules to probe domain structures in supported planar bilayers. These included BODIPY-labeled ganglioside, sphingomyelin, and three new cholesterol derivatives, as well as NBD-labeled phosphatidylcholine, sphingomyelin, and cholesterol. Interestingly, many fluorescent lipid probes, including derivatives of known raft-associated lipids, preferentially partitioned into topographical features consistent with nonraft domains. This suggests that the covalent attachment of a small fluorophore to a lipid molecule can abolish its ability to associate with rafts. In addition, the localization of one of the BODIPY-cholesterol derivatives was dependent on the lipid composition of the bilayer. These data suggest that conclusions about the identification of membrane domains in supported planar bilayers on the basis of fluorescent lipid probes alone must be interpreted with caution. The combination of AFM with fluorescence microscopy represents a more rigorous means of identifying lipid domains in supported bilayers.

INTRODUCTION

Lipid microdomains, or rafts, formed as a result of specific lipid-lipid or lipid-protein interactions in the cell membrane, are thought to play an important role in regulating signal transduction, cellular transport, and lipid sorting (1–8). Applying fluorescence microscopy or spectroscopy to study these structures and their dynamics in vivo is a challenge because of the lack of adequate imaging techniques with sufficient spatial and/or temporal resolution (9) as well as the limited number of specific lipid antibodies or lipid-binding protein domains that are available to serve as probes (10,11). Incorporating an artificial chromophore such as NBD, BODIPY, anthracene, pyrene, diphenylhexatriene, or a polyene chain into one of the fatty acid side chains is a common strategy to create fluorescent lipids to study metabolism, cellular transport, and distribution of lipids (12). The majority of these probes were introduced before the importance of lipid phase separation was recognized. Recently it has been demonstrated, using fluorescence quenching assays with model membranes (12–15), that chemical modification of a raft-associated lipid with a fluorophore can alter its ability to remain associated with (or associate to) these domains (15–17). In addition, correlated atomic force-fluorescence microscopic methods have recently shown promise in visualizing microdomains and fluorescence probe distribution simultaneously (18–21), including the effect of extrinsic markers on the morphology of lipid monolayers (22). This study was motivated by the realization that atomic force microscopy (AFM) can detect membrane microdomains using the differences in height between lipids existing in different phase regimes (20,23–26), including rafts or liquid-ordered (l_o) phases reported to be ~0.5–1 nm above the surrounding liquid-disordered (l_d) phase in model membranes composed of DOPC/sphingomyelin (SM)/cholesterol (Chl) (27–31). Herein we describe the use of simultaneous coupled AFM-confocal imaging to investigate the ability of the various lipids such as ganglioside G_{M1}, phosphatidylcholine, SM, and Chl labeled with NBD or BODIPY, to partition into the l_o or l_d domains of phase-segregated planar lipid bilayers. Our findings demonstrate that correlated AFM/fluorescence microscopy is a simple approach for identifying the preferential localization of fluorescent lipid probes. The attachment of a fluorophore such as NBD or BODIPY on the acyl chain of a saturated lipid or of Chl generally decreases the affinity of the lipid or sterol for the more ordered domains.

MATERIALS AND METHODS

Materials

N-stearoyl-D-*erythro*-sphingosylphosphorylcholine (synSM, 18:0), 1,2-dioleoyl-*sn*-glycerol-3-phosphocholine (DOPC, 18:1), brain bovine G_{M1} ammonium salt (brain G_{M1}), 1-palmitoyl-2-(6-[(7-nitro-2-1,3-benzoxadiazol-4-yl)amino]hexanoyl)-*sn*-glycero-3-phosphocholine (NBD-PC) (Fig. 1 *A*), 25-(*N*-[(7-nitro-2-1,3-benzoxadiazol-4-yl)methyl] amino]-27-norcholesterol

Submitted August 29, 2005, and accepted for publication November 23, 2005.

Address reprint requests to C. M. Yip, Tel.: 416-978-7853; Fax: 416-978-4317; E-mail: christopher.yip@utoronto.ca.

0006-3495/06/03/2170/09 $2.00

doi: 10.1529/biophysj.105.073510

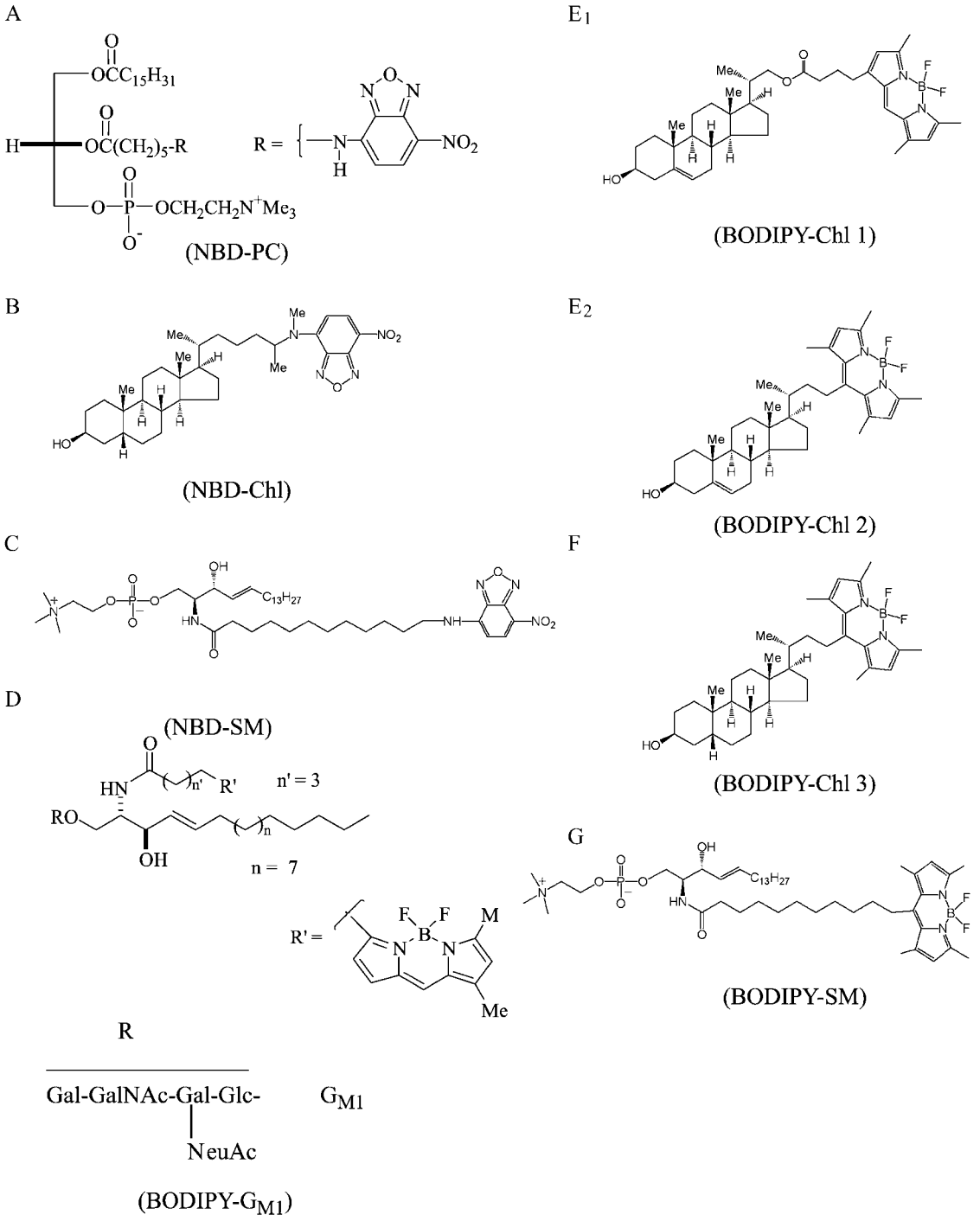

FIGURE 1 Chemical structures of (*A*) NBD-PC, (*B*) NBD-Chl, (*C*) NBD-SM, (*D*) BODIPY-G_{M1}, (E_1 and E_2) BODIPY-Chl 1 and 2, (*F*) BODIPY-Chl 3, and (*G*) BODIPY-SM.

(NBD-Cholesterol) (Fig. 1 *B*), and *N*-(12-[(7-nitro-2-1,3-benzoxadiazol-4-yl)amino)dodecanoyl]sphingosine-1-phosphocholine (NBD-SM) (Fig. 1 *C*) were purchased from Avanti Polar Lipids (Alabaster, AL). Chl was purchased from Sigma-Aldrich Canada (Oakville, ON, Canada). BODIPY FL C5-ganglioside G_{M1} (BODIPY-G_{M1}) (Fig. 1 *D*) and Alexa Fluor 555 cholera toxin subunit B (Alexa555-CTX-B) were purchased from Invitrogen Canada (Burlington, ON, Canada). BODIPY-Chl analogs (1, 2, and 3) (Fig. 1, E_1, E_2, and *F*) were synthesized as described (Z. Li, E. Mintzer, and R. Bittman, unpublished). BODIPY-SM (Fig. 1 *G*) was synthesized by *N*-acylation of sphingosylphosphorylcholine with a *p*-nitrophenyl ester of a BODIPY-fatty acid conjugate.

Liposome preparation

The liposomes were prepared by dissolving the required amounts of the various lipids in chloroform or chloroform/methanol (2:1), removing the

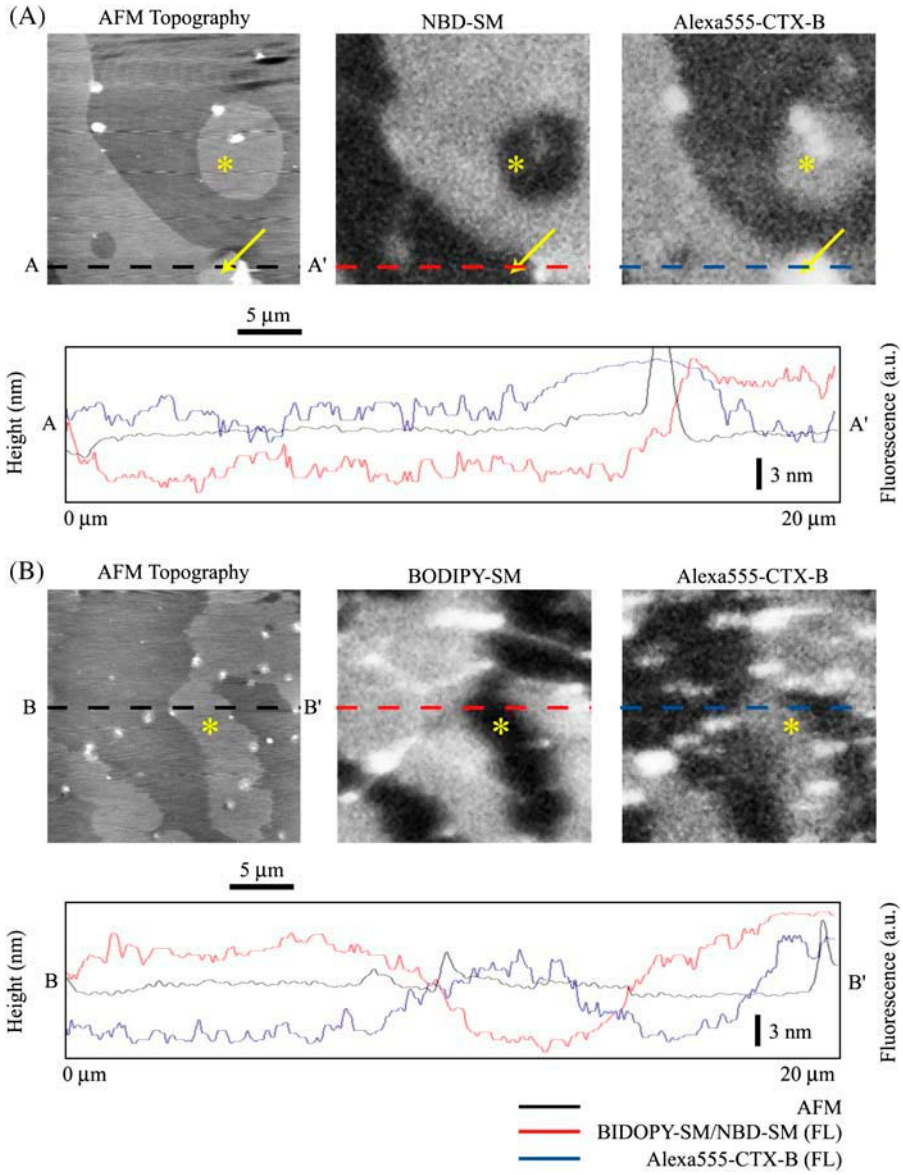

FIGURE 2 Simultaneous AFM-confocal imaging of reconstituted rafts in model SPBs composed of 34 mol % DOPC/34 mol % synSM (C18)/30 mol % Chl/2 mol % brain G_{M1} with (*A*) 0.2% NBD-SM or (*B*) 0.2 mol % BODIPY-SM. Alexa555-CTX-B was added to locate the ganglioside receptor G_{M1}, a raft-associated lipid. (*Inset*) Corresponding section analysis along A-A′ and B-B′.

solvent by rotary evaporation and keeping the films under vacuum for 3–4 h to remove occluded solvent. The lipid films were hydrated with 10 mM HEPES buffer containing 150 mM NaCl at pH 7.4 to a final lipid concentration of ~1 mM. Unilamellar vesicles were formed by sonication in a heated ultrasonic cleaner (~60°C) until the suspension became clear or only slightly hazy.

Supported planar bilayer preparation

Supported planar bilayers (SPBs) were formed by in situ fusion of 100 μl of 1 mM liposome suspension containing the desired lipid composition and 400 μl of 10 mM HEPES buffer, pH 7.4, containing 4 mM $CaCl_2$, 150 mM NaCl, onto a freshly cleaved mica disc (~25 mm in diameter and ~0.17 mm in thickness) held in a custom-made open fluid cell. The liposomes were first allowed to fuse at ambient temperature for 3 min, heated in place to 70°C for 3 min, and then allowed to cool to room temperature. This heating-cooling step facilitated the nucleation and growth of micron-size gel-phase domains, as has been reported by others (32). This preparation step was performed in place on the AFM-confocal-total internal reflection fluorescence (TIRF) instrument, as described in the following section.

Coaxial confocal-AFM imaging

All imaging was performed using an integrated AFM-confocal-TIRF imaging system. In this system, a confocal microscope (FluoView 500, Olympus, Melville, NY) was combined into a single imaging platform with an atomic force microscope (Nanoscope IIIa Bioscope, Digital Instruments/Veeco, Santa Barbara, CA) through an Olympus IX70 inverted microscope base. All confocal images were acquired using an Olympus 60× TIRF objective (NA ~ 1.45). SPBs were formed in situ as described earlier. The fluid cell was washed sequentially with pH 7.4 buffers containing 10 mM HEPES, 4 mM $CaCl_2$, 150 mM NaCl, followed by 10 mM HEPES, 4 mM EDTA, 150 mM NaCl, and finally 10 mM HEPES, 150 mM NaCl to remove excess solution liposomes before confocal-AFM imaging. All procedures were performed in the dark to avoid photobleaching of the fluorophores. Once the formation of the SPB was confirmed by AFM and confocal imaging, for some experiments a small volume of concentrated Alexa555 CTX-B stock solution (~1 mg/ml) was injected into the custom-designed open fluid cell, allowing it to distribute evenly by diffusion. From the total quantity of the toxin injected and the total cell volume immediately after injection, the final concentration of CTX-B was estimated to be ~1 μg/ml. All BODIPY- and

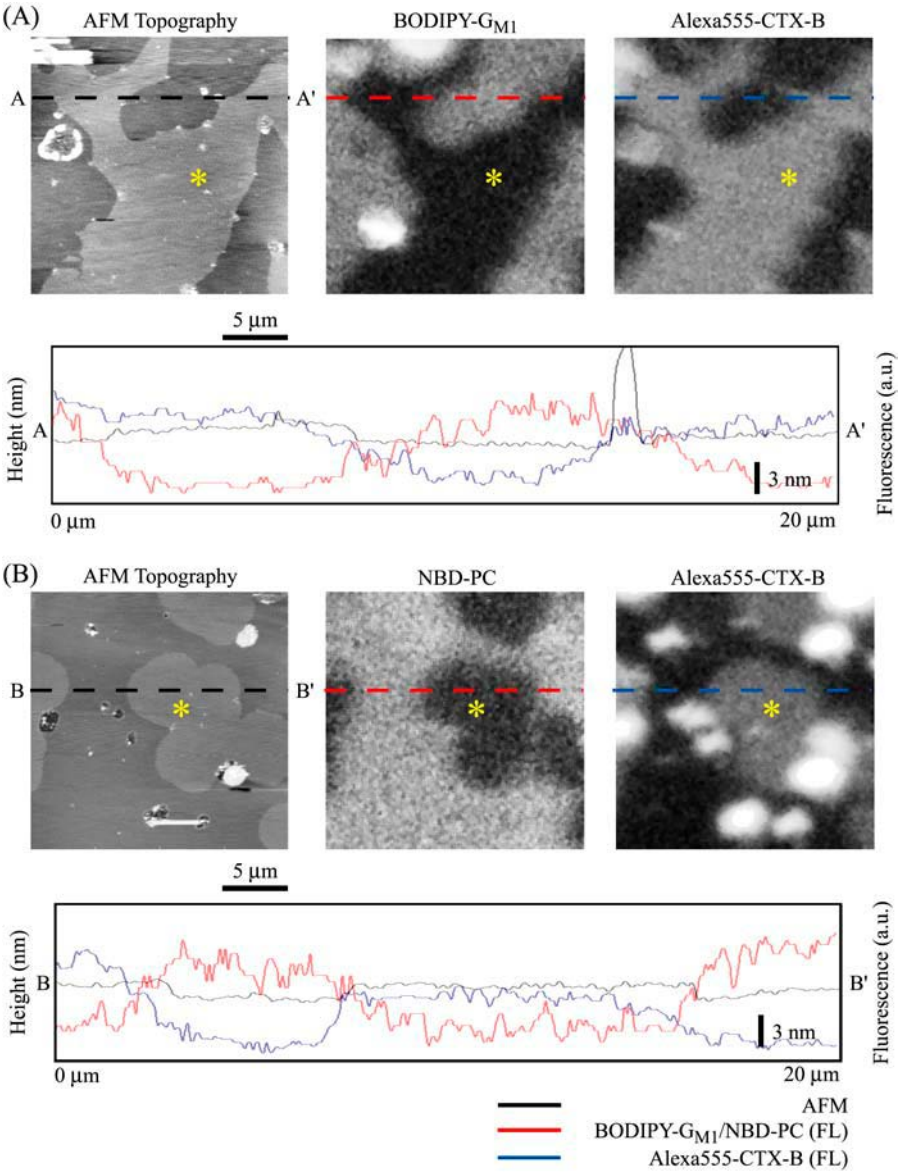

FIGURE 3 Simultaneous AFM-confocal imaging of reconstituted rafts in model SPBs composed of 34 mol % DOPC/34 mol % SynSM (C18)/30 mol % Chl/2 mol % brain G_{M1} with (*A*) 0.2 mol % BODIPY-G_{M1} or (*B*) 0.2 mol % NBD-PC. Alexa555-CTX-B was added to locate the ganglioside receptor G_{M1}, a raft-associated lipid. (*Inset*) Corresponding section analysis along A-A′ and B-B′.

NBD-containing compounds were excited by an Ar-ion 488 nm laser, and the emission was collected using a photomultiplier tube (PMT) fitted with a 510–525 nm band-pass filter. A 543 nm HeNe laser was used to excite the Alexa555 fluorophores, and the Alexa555 fluorescence was captured using another PMT equipped with a 560-nm high-pass filter. Confocal pinholes for both PMTs were set at 800 μm to maximize fluorescence counts emitted by the fluorophores. The BODIPY/NBD and Alexa555 fluorophores were sequentially excited to minimize possible cross talk between the BODIPY/NBD and Alexa555 PMT channels.

Although the fluorescence and AFM images are collected simultaneously, there are differences in the timescale of imaging and the actual area being imaged by the two techniques. The AFM data were collected as 512 × 512 pixel 16-bit images at a typical line scan rate of 1.2 Hz, whereas the 1024 × 1024 pixel 12-bit confocal images were acquired at a line scan rate of ~105 Hz. It is also important to note that the region imaged by the AFM is a subset of the confocal microscope's field of view. This is a result of the limited (~125 μm × ~125 μm) scan window afforded the AFM scanner compared with the much larger field of view provided by the 60× objective used by the confocal microscope.

Image analysis

AFM image analysis was conducted using the Digital Instruments Nanoscope software (version 4.42r9). Height images were flattened and plane-fit in the x-scan direction. Quantitative height measurements were determined by section analysis and shown as an average of 50 measurements. Contrast adjustments for the fluorescent images were made using ImagePro Plus (version 4.5, Silver Spring, MD) or the public domain program ImageJ (developed at the U.S. National Institutes of Health and available on the Internet at http://rsb.info.nih.gov/ij). AFM-confocal image correlation was accomplished using Adobe Photoshop or custom in-house developed Java software.

RESULTS AND DISCUSSION

Binding of cholera toxin to G_{M1}

Simultaneous AFM-confocal imaging at ambient temperature (~23°C) revealed that SPBs containing 1:1 DOPC/SM/30

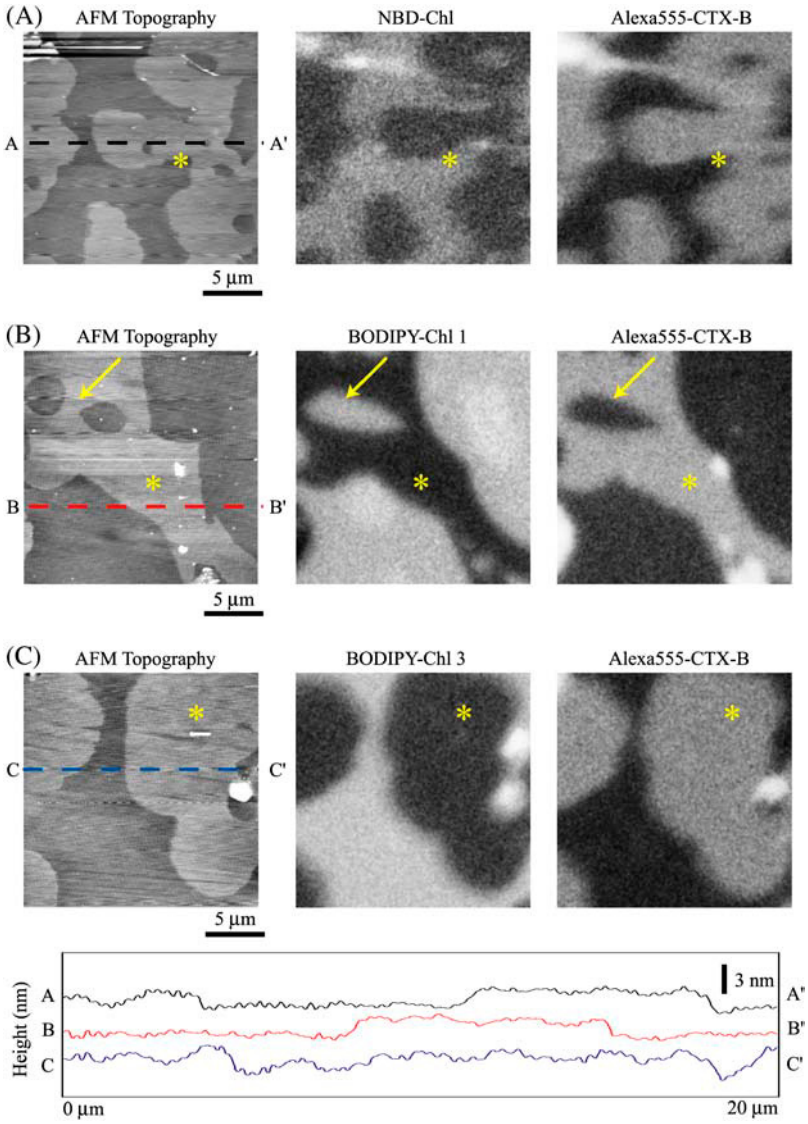

FIGURE 4 Simultaneous AFM-confocal imaging of reconstituted rafts in model SPBs composed of 34 mol % DOPC/34 mol % SynSM (C18)/28 mol % Chl/2 mol % brain G_{M1} with (*A*) 2 mol % NBD-Chl, (*B*) 34 mol % DOPC/34 mol % SynSM (C18)/30 mol % Chl/2 mol % brain GM1 with 0.2 mol % BODIPY-Chl 1, or (*C*) 0.2 mol % BODIPY-Chl 3. Alexa555-CTX-B was added to locate the ganglioside receptor G_{M1}, a raft-associated lipid. (*Inset*) Corresponding section analysis along A-A′, B-B′, and C-C′ in the AFM topography images.

mol % Chl/2 mol % brain G_{M1} formed phase-segregated high (l_o) and low (l_d) domains with an average height difference of ~1 nm, regardless of the type of exogenous SM (synSM, 18:0 or 16:0, or brain SM) or fluorescently labeled component. Not unexpectedly, we were unable to resolve the individual G_{M1} molecules by AFM. This is likely a consequence of the flexibility of the G_{M1} headgroup. Accordingly, to visualize the G_{M1}-containing domains, the B-subunit of CTX-B, labeled with Alexa555, was introduced into the AFM fluid cell.

It is well known that CTX-B binds to the G_{M1} headgroup to form, depending on the local G_{M1} concentration, well-ordered two-dimensional crystalline arrays extending ~2.5 nm in height above G_{M1}-containing domains (18,19,33). Although our correlated AFM/confocal imaging confirmed that Alexa555-CTX-B was associated with the higher domains, we were unable to resolve the individual CTX-B molecules by topography imaging, nor was the expected increase in height attributable to association of the labeled CTX-B to the G_{M1} molecules in the l_o domains detected. This is likely a consequence of the low ~2 mol % brain G_{M1} in the l_o domains and incomplete coverage by CTX-B as a densely packed two-dimensional monolayer. However, we were able to resolve a direct spatial correspondence between fluorescence intensity and the l_o domains, as identified by in situ AFM (see *yellow arrows* in Fig. 2 *A*).

BODIPY-SM and NBD-SM preferentially partition into the l_d domains

A consequence of its long alkyl chains and corresponding high melting temperatures, SM is expected to be colocalized with the taller G_{M1}-containing high domains, a model that has been supported by x-ray diffraction studies (34). Surprisingly, our correlated AFM/confocal imaging revealed that BODIPY and NBD analogs of SM in fact preferentially localize in the lower (l_d) domains (Fig. 2). In the BODIPY

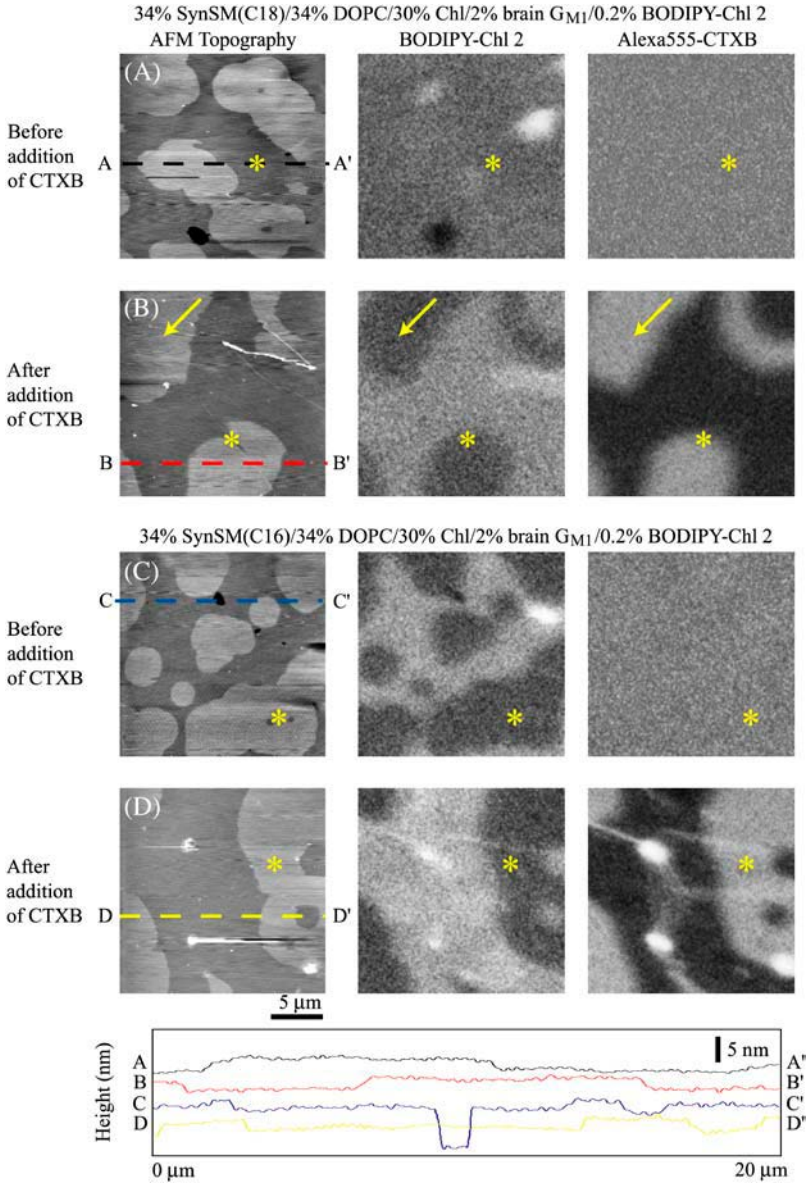

FIGURE 5 Simultaneous AFM-confocal imaging of reconstituted rafts in model SPBs composed of (*A–B*) 34 mol % SynSM (C18)/34 mol % DOPC/30 mol % Chl/2 mol % brain G_{M1} with 0.2 mol % BODIPY-Chl 2 or (*C–D*) 34 mol % SynSM (C16)/34 mol % DOPC/30 mol % Chl/2 mol % brain G_{M1} with 0.2 mol % BODIPY-Chl 2. Alexa555-CTX-B was added to locate the ganglioside receptor G_{M1}, a raft-associated lipid. (*Inset*) Corresponding section analysis along A-A′, B-B′, C-C′, and D-D′ in the AFM topography images.

and NBD-labeled lipids, one of the fatty acyl chains was replaced with an NBD- or BODIPY-labeled acyl chain. A recent study using a headgroup-labeled BODIPY-G_{M1} revealed that it failed to enter a more ordered gel domain, whereas a headgroup labeled Alexa488-G_{M1} preferentially partitioned into the gel domain (19). These data strongly suggest that phase partitioning of fluorophores between domains is a complex phenomenon that depends not only on the site of fluorophore attachment but also on the physical properties of the fluorophore.

BODIPY-G_{M1} and NBD-PC preferentially partition into the l_d domains

Simultaneous AFM-confocal imaging at ambient temperature (~23°C) revealed that SPBs containing 1:1 DOPC/synSM, 18:0/30 mol % Chl/2 mol % brain G_{M1}/0.2 mol % BODIPY-G_{M1} and 0.2 mol % of NBD-PC, phase-segregated into high (l_o) and low (l_d) domains with height difference ranging from ~0.5 to 1.5 nm, in agreement with previous AFM and x-ray diffraction studies (28–30,33). NBD-PC is known to partition into l_d phase (32,34–36), whereas CTX-B is known to strongly associate with the ganglioside G_{M1} (34). Close inspection revealed that the green fluorescence arising from the BODIPY and NBD labels was predominately localized to the low domains (l_d), whereas the red fluorescence associated with Alexa555 labeled CTX-B remained mainly associated with the tall (l_o) domains (Fig. 3). Our data suggest that brain G_{M1} preferentially segregates to the tall (l_o) domains, whereas BODIPY-G_{M1} localizes preferentially in the nonraft domains. One would expect that there would be some binding of CTX-B to the low domain because of the

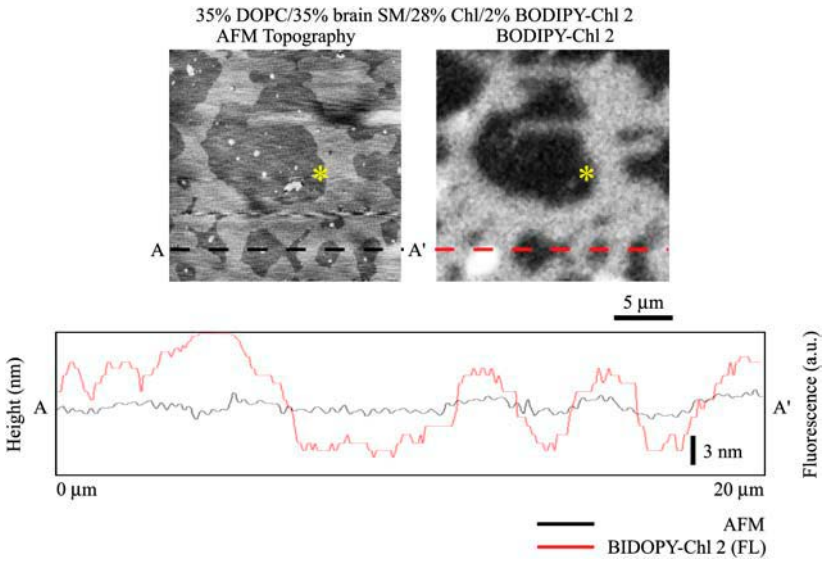

FIGURE 6 Simultaneous AFM-confocal imaging of reconstituted rafts in model SPBs composed of 35 mol % DOPC/35 mol % brain SM/28 mol % Chl/2 mol % BODIPY-Chl 2. (*Inset*) Corresponding section analysis along A-A′.

presence of the BODIPY G_{M1}; however, the relative fluorescence intensity of CTX-B would be much higher in the high domain because of the 10-fold higher content of brain G_{M1} (the molar ratio of brain G_{M1}/BODIPY G_{M1} is 10:1, in this case). Although CTX-B is known to induce clustering of G_{M1} (37–39), it is not likely that the introduction of CTX-B would result in the translocation of BODIPY-G_{M1} from the low to high domains. Thus, this Alexa555-CTX-B labeling experiment demonstrates that the unmodified G_{M1} sequesters into the high domains as expected; however, it also clearly reveals that BODIPY-G_{M1} unexpectedly associates with the lower, nonraft, domains (Fig. 3).

Domain partitioning of fluorescently labeled cholesterol

A major constituent of eukaryotic membranes, Chl plays a critical role in defining membrane structure and function (40), including regulating lipid trafficking and sorting (41). Our correlated AFM-fluorescence data clearly reveal that NBD-Chl and BODIPY-Chl 1 and 3 do not distribute preferentially in the l_o phase (Fig. 4), which is enriched in Chl and sphingolipids (8). The side chain of Chl resides in the bilayer interior (40,42); however, the NBD group, which is generally considered to reside deep in the bilayer (43), was reduced when a water-soluble reducing agent (dithionite) was added to NBD-Chl-containing bilayers (44), indicating that the NBD moiety at C25 of Chl can loop back toward the lipid/water interface. Our study agrees with a recent finding that NBD-Chl (45) does not mimic Chl (44,46).

BODIPY-Chl 3 is an analog of coprostanol. Although structurally related to Chl, this analog was designed not to mimic Chl, but to serve as a nonraft probe. Since the sterol nucleus is not flat in BODIPY-Chl 3, this compound would differ from natural Chl with respect to lipid-lipid interactions, consistent with the results from this study.

BODIPY-Chl 2 is a more faithful mimic of Chl since it retains the planar conformation of the Chl ring system and does not contain any polar atoms linking BODIPY to the sterol ring. This is in agreement with our findings that BODIPY-Chl 2 partitions into a Triton X-100 low density insoluble fraction, whereas BODIPY-Chl 3 does not (47). Nevertheless, the localization of BODIPY-Chl 2 within the bilayer is dependent on the type of SM used to form the SPBs. For instance, BODIPY-Chl 2 distributes uniformly across the higher (l_o) and the lower (l_d) domains in bilayers containing synSM 18:0. As shown in Fig. 5 *A*, binding of Alexa555-CTX-B induced quenching of BODIPY fluorescence at the higher (l_d) domains. Sequestering of BODIPY dyes or resonance energy transfer between BODIPY and Alexa555 are possible mechanisms that can result in localized quenching of BODIPY fluorescence. The exact mechanisms remain unclear. In contrast, BODIPY-Chl 2 preferentially partitioned into the lower domains in the bilayers containing synSM 16:0 (Fig. 5 *B*) and preferentially localized in the higher (l_o) domains in bilayers containing brain SM (Fig. 6).

The higher hydrophobicity of BODIPY relative to NBD allows for better insertion into the bilayer (17,48). However, this does not guarantee that a BODIPY-bearing lipid would preferentially partition into the more ordered (l_o) phase, as shown by the behavior of BODIPY-GM1 and BODIPY-SM. Different linkers that connect the BODIPY and the sterol side chain result in differences among BODIPY-Chl analogs. The linker coupling BODIPY to the sterol in BODIPY-Chl 1 contains an ester functionality, whereas in BODIPY-Chl 2 a short linker devoid of oxygen atoms was employed. Interestingly, a relatively small change in structure from BODIPY-Chl-1 to BODIPY-Chl-2 can change the location of the sterol. The sensitivity of the domain partitioning of BODIPY-Chl 2 to the nature of the surrounding lipid is illustrated by the change caused by the nature of the SM (Figs. 5 and 6).

IMPLICATIONS AND CONSIDERATIONS

Although our confocal images show significant contrast associated with the segregation of the dyes into different spatial domains, it should be noted that the fluorescence intensity in the two domains depends not only on the concentration of the fluorophore in that domain, but also on its quantum yield in that particular domain. We have not quantitatively determined the partition coefficient of the dyes examined in our studies, but rather used the correlated AFM approach to assign and assess the phases that the dyes are in favor of staining. Using planar supported lipid bilayers to study membrane or protein-membrane dynamics and interactions allows us to systematically vary lipid composition and to employ the correlated AFM-confocal approach with very little ambiguity in the results. Planar supported lipid bilayers lack membrane curvatures that are present in the spherical model membranes such as giant unilamellar vesicles (GUVs) or cell membranes. However, it has been demonstrated that GUVs partition into liquid/liquid immiscible domains in the same way that planar supported lipid bilayers do, and the lipids in both leaflets of the supported bilayers are freely mobile (49).

CONCLUSIONS

Our studies have several important implications. Upon conjugation with NBD or BODIPY, the lipids examined in this study with the exception of BODIPY-Chl 2, and that had been shown to associate with raft domains in the absence of the fluorophore no longer preferentially segregated to the taller raft domains. This is consistent with previous reports (12,15). Topographical AFM can provide details of the physical structure of the domains where the fluorescent probes are preferentially located. This correlated approach is an excellent means of investigating the partitioning of fluorescent probes in a coexisting raft/nonraft system. In addition, this study illustrates the possible adverse effects arising from the use of NBD- and BODIPY-labels to identify raft domains.

This work was supported by the Canadian Institutes of Health Research (R.M.E.: MA-7654; C.M.Y.: MT:14769) and the Natural Sciences and Engineering Research Council of Canada (C.M.Y.: 194435). C.M.Y. acknowledges support from the Canada Research Chairs program, the Canadian Foundation for Innovation, the Ontario Innovation Trust, and the Ontario Research and Development Challenge Fund.

REFERENCES

1. Bacia, K., D. Scherfeld, N. Kahya, and P. Schwille. 2004. Fluorescence correlation spectroscopy relates rafts in model and native membranes. *Biophys. J.* 87:1034–1043.
2. Chini, B., and M. Parenti. 2004. G-protein coupled receptors in lipid rafts and caveolae: how, when and why do they go there? *J. Mol. Endocrinol.* 32:325–338.
3. Golub, T., S. Wacha, and P. Caroni. 2004. Spatial and temporal control of signaling through lipid rafts. *Curr. Opin. Neurobiol.* 14:542–550.
4. Hammond, A. T., F. A. Heberle, T. Baumgart, D. Holowka, B. Baird, and G. W. Feigenson. 2005. Crosslinking a lipid raft component triggers liquid ordered-liquid disordered phase separation in model plasma membranes. *Proc. Natl. Acad. Sci. USA.* 102:6320–6325.
5. Mukherjee, S., and F. R. Maxfield. 2004. Membrane domains. *Annu. Rev. Cell Dev. Biol.* 20:839–866.
6. Pierce, S. K. 2004. To cluster or not to cluster: FRETting over rafts. *Nat. Cell Biol.* 6:180–181.
7. Pike, L. J. 2004. Lipid rafts: heterogeneity on the high seas. *Biochem. J.* 378:281–292.
8. Simons, K., and W. L. Vaz. 2004. Model systems, lipid rafts, and cell membranes. *Annu. Rev. Biophys. Biomol. Struct.* 33:269–295.
9. Simons, K., and D. Toomre. 2000. Lipid rafts and signal transduction. *Nat. Rev. Mol. Cell Biol.* 1:31–39.
10. Ishitsuka, R., A. Yamaji-Hasegawa, A. Makino, Y. Hirabayashi, and T. Kobayashi. 2004. A lipid-specific toxin reveals heterogeneity of sphingomyelin-containing membranes. *Biophys. J.* 86:296–307.
11. Maier, O., V. Oberle, and D. Hoekstra. 2002. Fluorescent lipid probes: some properties and applications (a review). *Chem. Phys. Lipids.* 116: 3–18.
12. Kuerschner, L., C. S. Ejsing, K. Ekroos, A. Shevchenko, K. I. Anderson, and C. Thiele. 2004. Polyene-lipids: a new tool to image lipids. *Nat. Methods.* 2:39–45.
13. Ahmed, S. N., D. A. Brown, and E. London. 1997. On the origin of sphingolipid/cholesterol-rich detergent-insoluble cell membranes: physiological concentrations of cholesterol and sphingolipid induce formation of a detergent-insoluble, liquid-ordered lipid phase in model membranes. *Biochemistry.* 36:10944–10953.
14. London, E., and G. W. Feigenson. 1981. Fluorescence quenching in model membranes. 1. Characterization of quenching caused by a spin-labeled phospholipid. *Biochemistry.* 20:1932–1938.
15. Wang, T. Y., and J. R. Silvius. 2000. Different sphingolipids show differential partitioning into sphingolipid/cholesterol-rich domains in lipid bilayers. *Biophys. J.* 79:1478–1489.
16. Chattopadhyay, A. 1990. Chemistry and biology of N-(7-nitrobenz-2-oxa-1,3-diazol-4-yl)-labeled lipids: fluorescent probes of biological and model membranes. *Chem. Phys. Lipids.* 53:1–15.
17. Kaiser, R. D., and E. London. 1998. Determination of the depth of BODIPY probes in model membranes by parallax analysis of fluorescence quenching. *Biochim. Biophys. Acta.* 1375:13–22.
18. Burns, A. R. 2003. Domain structure in model membrane bilayers investigated by simultaneous atomic force microscopy and fluorescence imaging. *Langmuir.* 19:8358–8363.
19. Burns, A. R., D. J. Frankel, and T. Buranda. 2005. Local mobility in lipid domains of supported bilayers characterized by atomic force microscopy and fluorescence correlation spectroscopy. *Biophys. J.* 89: 1081–1093.
20. Hollars, C. W., and R. C. Dunn. 1998. Submicron structure in L-alpha-dipalmitoylphosphatidylcholine monolayers and bilayers probed with confocal, atomic force, and near-field microscopy. *Biophys. J.* 75: 342–353.
21. Shaw, J. E., A. Slade, and C. M. Yip. 2003. Simultaneous in situ total internal reflectance fluorescence/atomic force microscopy studies of DPPC/dPOPC microdomains in supported planar lipid bilayers. *J. Am. Chem. Soc.* 125:11838–11839.
22. Merritt, E. A., T. K. Sixma, K. H. Kalk, B. A. van Zanten, and W. G. Hol. 1994. Galactose-binding site in Escherichia coli heat-labile enterotoxin (LT) and cholera toxin (CT). *Mol. Microbiol.* 13:745–753.
23. Yang, X. M., D. Xiao, S. J. Xiao, and Y. Wei. 1994. Domain structures of phospholipid monolayer Langmuir-Blodgett films determined by atomic force microscopy. *Appl. Phys. A.* 59:139–143.
24. Yang, X. M., D. Xiao, S. J. Xiao, Z. H. Lu, and Y. Wei. 1994. Observation of chiral domain morphology in a phospholipid Langmuir-Blodgett monolayer by atomic-force microscopy. *Phys. Lett. A.* 193:195–198.
25. Masai, J., T. Shibata-Seki, K. Sasaki, H. Murayama, and K. Sano. 1996. Scanning force microscopy characterization of thin lipid films on a substrate. *Thin Solid Films.* 273:289–296.

26. Hollars, C. W., and R. C. Dunn. 1997. Submicron fluorescence, topology, and compliance measurements of phase-separated lipid monolayers using tapping-mode near-field scanning optical microscopy. *J. Phys. Chem. B*. 101:6313–6317.

27. Yuan, C., J. Furlong, P. Burgos, and L. J. Johnston. 2002. The size of lipid rafts: an atomic force microscopy study of ganglioside GM1 domains in sphingomyelin/DOPC/cholesterol membranes. *Biophys. J*. 82:2526–2535.

28. Saslowsky, D. E., J. Lawrence, X. Ren, D. A. Brown, R. M. Henderson, and J. M. Edwardson. 2002. Placental alkaline phosphatase is efficiently targeted to rafts in supported lipid bilayers. *J. Biol. Chem.* 277:26966–26970.

29. Rinia, H. A., M. M. Snel, J. P. van der Eerden, and B. de Kruijff. 2001. Visualizing detergent resistant domains in model membranes with atomic force microscopy. *FEBS Lett*. 501:92–96.

30. Milhiet, P. E., M. C. Giocondi, O. Baghdadi, F. Ronzon, B. Roux, and C. Le Grimellec. 2002. Spontaneous insertion and partitioning of alkaline phosphatase into model lipid rafts. *EMBO Rep*. 3:485–490.

31. Dietrich, C., L. A. Bagatolli, Z. N. Volovyk, N. L. Thompson, M. Levi, K. Jacobson, and E. Gratton. 2001. Lipid rafts reconstituted in model membranes. *Biophys. J*. 80:1417–1428.

32. McKiernan, A. E., T. V. Ratto, and M. L. Longo. 2000. Domain growth, shapes, and topology in cationic lipid bilayers on mica by fluorescence and atomic force microscopy. *Biophys. J*. 79:2605–2615.

33. Gandhavadi, M., D. Allende, A. Vidal, S. A. Simon, and T. J. McIntosh. 2002. Structure, composition, and peptide binding properties of detergent soluble bilayers and detergent resistant rafts. *Biophys. J*. 82:1469–1482.

34. Worthman, L. A., K. Nag, P. J. Davis, and K. M. Keough. 1997. Cholesterol in condensed and fluid phosphatidylcholine monolayers studied by epifluorescence microscopy. *Biophys. J*. 72:2569–2580.

35. Akamatsu, S., O. Bouloussa, K. W. To, and F. Rondelez. 1992. Two-dimensional dendritic growth in Langmuir monolayers of D-myristoyl alanine. *Phys. Rev. A*. 46:R4504–R4507.

36. Knobler, C. M. 1990. Seeing phenomena in flatland—studies of monolayers by fluorescence microscopy. *Science*. 249:870–874.

37. Antes, P., G. Schwarzmann, and K. Sandhoff. 1992. Detection of protein mediated glycosphingolipid clustering by the use of resonance energy transfer between fluorescent labelled lipids. A method established by applying the system ganglioside GM1 and cholera toxin B subunit. *Chem. Phys. Lipids*. 62:269–280.

38. Mitchell, J. S., O. Kanca, and B. W. McIntyre. 2002. Lipid microdomain clustering induces a redistribution of antigen recognition and adhesion molecules on human T lymphocytes. *J. Immunol*. 168: 2737–2744.

39. Nagy, P., G. Vereb, Z. Sebestyen, G. Horvath, S. J. Lockett, S. Damjanovich, J. W. Park, T. M. Jovin, and J. Szollosi. 2002. Lipid rafts and the local density of ErbB proteins influence the biological role of homo- and heteroassociations of ErbB2. *J. Cell Sci*. 115:4251–4262.

40. Bittman, R. 1997. Has nature designed the cholesterol side chain for optimal interactions with phospholipids? *In* Subcellular Biochemistry, Vol. 28: Cholesterol: Its Functions and Metabolism in Biology and Medicine. R. Bittman, editor. Plenum, New York. 145–171.

41. Hoekstra, D., and S. C. D. van IJzendoorn. 2000. Lipid trafficking and sorting: how cholesterol is filling gaps. *Curr. Opin. Cell Biol*. 12:496–502.

42. Wu, W. G., and L. M. Chi. 1991. Conformational change of cholesterol side-chain in lipid bilayers. *J. Am. Chem. Soc*. 113:4683–4685.

43. Chattopadhyay, A., and E. London. 1988. Spectroscopic and ionization properties of N-(7-Nitrobenz-2-Oxa-1,3-Diazol-4-Yl)-labeled lipids in model membranes. *Biochim. Biophys. Acta*. 938:24–34.

44. Scheidt, H. A., P. Muller, A. Herrmann, and D. Huster. 2003. The potential of fluorescent and spin-labeled steroid analogs to mimic natural cholesterol. *J. Biol. Chem*. 278:45563–45569.

45. Mukherjee, S., and A. Chattopadhyay. 2005. Monitoring cholesterol organization in membranes at low concentrations utilizing the wavelength-selective fluorescence approach. *Chem. Phys. Lipids*. 134:79–84.

46. Loura, L. M. S., A. Fedorov, and M. Prieto. 2001. Exclusion of a cholesterol analog from the cholesterol-rich phase in model membranes. *Biochim. Biophys. Acta*. 1511:236–243.

47. Li, Z., E. Mintzer, and R. Bittman. 2006. First synthesis of free cholesterol-BODIPY conjugates. *J. Org. Chem*. In press.

48. Asuncion-Punzalan, E., K. Kachel, and E. London. 1998. Groups with polar characteristics can locate at both shallow and deep locations in membranes: the behavior of dansyl and related probes. *Biochemistry*. 37:4603–4611.

49. Crane, J. M., and L. K. Tamm. 2004. Role of cholesterol in the formation and nature of lipid rafts in planar and spherical model membranes. *Biophys. J*. 86:2965–2979.